Model-Based Combustion Control to Reduce the Brake Specific Fuel Consumption and Pollutant Emissions under Real Driving Maneuvers

20XX-01-XXXX

Model-Based Combustion Control to Reduce the Brake Specific Fuel Consumption and Pollutant Emissions under Real Driving Maneuvers

Author, co-author (Do NOT enter this information. It will be pulled from participant tab in MyTechZone)

Affiliation (Do NOT enter this information. It will be pulled from participant tab in MyTechZone)

Abstract

The carbon footprint of the industrial economy is driving the engine manufacturers to lead the development of new technologies and fuels to lower pollutant and CO_2 emissions and that can be then shared with other industrial fields. Although battery electric equipment has already been introduced in the automotive field, diesel and gasoline vehicles are still widely used, thanks to the longer operating range, the faster refueling, and the lower cost. The transition towards new fuels and technologies can be guided by more efficient traditional internal combustion engines.

In this work, previously developed innovative piston damage and exhaust gas temperature models are coupled to manage the combustion process and thereby increasing the overall energy conversion efficiency. The piston erosion and the exhaust gas temperature at the turbine inlet are evaluated according to the models' estimation which manages both the spark advance, and lambda. In the first part of the paper, the previously developed exhaust gas temperature model is reversed and converted into a control function which is then implemented in a piston damage-based, spark advance controller. This controller targets a given piston erosion for a certain time, using more aggressive calibrations, thereby significantly increasing the combustion efficiency, and lowering the exhaust gas temperature, under knock-limited operating conditions. Furthermore, this decrease in exhaust gas temperature is converted into lowering the fuel enrichment with respect to the production calibrations. Moreover, the pollutant emissions associated to the production calibrations and those associated to the application of proposed controller are compared through a GT Power combustion model.

In the second part of the work, the complete controller is validated for both the transient and steady-state conditions, reproducing a real vehicle maneuver at the engine test bench. The results demonstrate that the combination of an accurate estimation of the damage induced by knock and the value of the exhaust gas temperature allows to reduce the brake specific fuel consumption by up to 20%. Moreover, the stoichiometric area of the engine operating field is extended by 20%, and the GT Power simulations show an average reduction of about 50% of the main pollutant species.

Keywords: combustion, efficiency, modeling, control, neural networks, energy management, control-oriented, knock, exhaust gas temperature, mixture enrichment, spark advance, lambda

Introduction

The CO_2 and pollutants emission limits for the automotive industry have been lowered with the aim of pushing manufacturers towards more efficient and sustainable technologies and fuels (synthetic fuels, vehicle electrification, innovative combustions, etc.) with lower environmental footprint [1].

So far, this trend has had a high effect on the research of light-duty engines and in this field the scenario is expected to further change soon. The efforts are driven to increase the energy conversion efficiency resulting in lower on-board energy consumption and pollutant emissions, thus reducing the greenhouse gas emissions and the extraction costs to address both the environmental and economic sustainability. The same considerations apply to other sectors (industry, railway, maritime, mining, genset) where heavy-duty engines are largely used. In this scenario, the research in the automotive field can lead the development of technologies that can be then shared with other industrial sectors [2].

In the last years, the research on internal combustion engines has focused a wide effort on the development of solutions to increase the combustion efficiency of gasoline engines. Modern Gasoline Direct Injection (GDI), turbo-charged (TC) engines represent the most suitable layout, thanks to their lower pollution levels and the different kinds of combustions (i.e., lean combustions, knocking and non-knocking conditions), that can be investigated to find new ways to manage and utilize 'dangerous' but more efficient combustions. Enabling knock-limited operating areas and accurately estimating the exhaust gas temperature at the turbine inlet are the most challenging fields for modern TC engines, due to the significant scope for improvements that can be achieved with an accurate and aware combustion control system. Indeed, knocking combustion [3, 4] and the maximum exhaust gas temperature at turbine inlet are the two main limits for the efficiency increase in the high speed and load region of the engine operating field, where the most used strategies are the Spark Advance (SA) degradation and the fuel mixture enrichment [5], known as component protection strategy. Nevertheless, these two actions cause an increase of both the fuel consumption and pollutant emissions. This topic is under the focus of powertrain manufacturers because the driving cycles for the vehicle homologation are becoming more aggressive, forcing the reduction of the component protection strategy, and extending the stoichiometric operating field of the engine [6, 7]. Several technologies have been developed during the last years such as the Variable Compression Ratio (VCR), the water injection and the usage of advanced materials for the turbine impeller [6, 7]. Moreover, the development of more-and-more sophisticated control strategies is currently a very interesting solution for engine manufacturers, because of the difficulties of finding innovative, reliable, and cost-effective functional technologies, especially in a time in which most of the resources are invested to develop new types of propulsion [8].

Considering the limits explained before for the efficiency increase, in literature, some works highlight the physical relationship between the knock intensity and the related piston erosion [9-12], but no combustion control strategies based on a modelled damage index can be found. On the other hand, control-oriented models that can accurately estimate the exhaust gas temperature on the entire engine operating field are a strategic tool to prevent turbine failure and maximize the conversion efficiency of the after-treatment system, as highlighted by Fu and Chen [13]. Nevertheless, a few examples of Real-Time (RT) models able to estimate the inlet turbine temperature are present in literature. One of the proposed algorithms is the one developed by Fulton and Van Nieuwstadt [14], which is based on the

estimation of the exhaust gas temperature at the turbine inlet with an open loop chain and a closed loop contribution which uses the signal of a thermocouple placed at the turbine outlet. However, this kind of sensor or different types (such as the resistance temperature detectors) are not used for the final on-vehicle application for cost and reliability reasons. Thus, other methods have been implemented for the exhaust gas temperature estimation, such as exploiting sensors installed on the final on-board application as the Universal Exhaust Gas Oxygen (UEGO) ones. Indeed, heaters of lambda (λ) sensors can be used to evaluate the exhaust gas temperature by analyzing the shape of the duty cycle signal, with which current flux to the heating element is controlled in order to compensate the effect of the surrounding exhaust gas on the measurement [15, 16, 17]. Applying this approach, the electrical heating power supplied to the sensor depends on the temperature, thus it is possible to estimate the temperature of the exhaust gases. Considering these analyses, it can be understood the importance of also implementing model-based approaches for the calculation of the desired quantity.

In this work, a model-based, combustion control system that manages both the SA and the target λ value is developed and validated. The SA control system includes a piston damage-based controller previously developed by the authors that determines the SA needed to reach a given piston erosion induced by knocking events in a certain time [18, 19], called damage speed. The λ control system is based on a reversed exhaust gas temperature model previously developed by the authors in [20, 21]. The proposed model is based on an algorithm to estimate the Temperature at the Exhaust Valve Opening (TEVO), that implements a custom closed valves analysis optimization algorithm [20, 21]. In a previous work of the authors [21], the exhaust gas temperature model is used for the offline optimization of the SA and the target λ maps to operate the engine under knock-limited conditions and with the maximum admissible temperature at the turbine inlet, demonstrating that the efficiency can be improved of 15% with respect to the production calibrations of the engine.

In this work two main aspects of novelty are introduced. The first is that the exhaust gas temperature algorithm proposed in [21] is reversed and coupled with a piston damage-based SA controller obtaining a complete SA-λ combustion controller that is implemented in a Rapid Control Prototyping (RCP) system used to directly control the combustion. The second aspect of novelty is that the Feedforward Neural Networks (FNN) algorithm, that is used to calculate the combustion phase index in the exhaust gas temperature model, can be used to build robust combustion control systems. Indeed, in the automotive field, these kinds of models are mainly used for modelling applications, such as for the prediction of the combustion phase [22, 23], the knocking events [24, 25], the pollutant emissions [26, 27] and the engine thermal behavior [28, 29].
With the proposed controller, the two main limits to the combustion efficiency increase for GDI TC engines are overtaken through the accurate calculation of the indexes that represent the actual intensity of the phenomena that have to be controlled: the piston erosion speed (the damage for a certain period of time) and the exhaust gas temperature at the turbine inlet.

The developed combustion control system is tested offline with a Software in the Loop (SiL) approach, using a control-oriented engine simulator developed by the authors in [30] that can simulate the instantaneous values of the main combustion indexes for a GDI TC engine, such as the crank angle degree of 50 % of mass fraction burned (MFB50), the maximum in-cylinder pressure (PMAX), the Maximum Amplitude of Pressure Oscillation (MAPO) and the exhaust gas temperature at the turbine inlet. After the offline validation, the complete algorithm is deployed in the RCP system and it is tested both under steady-state conditions, carrying out a power curve, and under transient conditions, reproducing at the test bench a real driving maneuver recorded on the vehicle. Then, the engine efficiency increase is evaluated comparing the Brake Specific Fuel Consumption (BSFC) measured during these tests with the reference values, represented by the value recorded during the same maneuver performed with the production calibrations of SA and λ.

In this work, the effects on the pollutant emissions production obtained managing the combustion with the proposed control system are also evaluated. Since no instruments for the pollutant emission measurements are present in the experimental setup, a GT Power combustion model referring to the average cylinder of the studied engine is calibrated. A two-zones Wiebe-based combustion model is developed with a closed valves analysis to match the average experimental in-cylinder pressure curve measured for each operating condition tested. This allows the estimation of the NOx and CO emissions thanks to kinetical models [31, 32]. It is important to highlight that the other pollutant emissions such as the HC are not calculated because predictive combustion models are required, that need specific geometrical features of the tested engine which are not available. The simulated NOx and CO values are used to train two FNN algorithms obtaining equivalent models that need a lower computational effort. This tool allows to simulate the concentration of the main pollutant emissions at the exhaust valve opening using the main engine parameters measured during tests carried out at the test bench.

In the final part of this work the developed SA-λ control system is used to directly manage the engine combustion during transient tests, evaluating the pollutant emissions at the engine out brought by the implementation of the proposed controller. A maximum reduction of 20% of the BSFC and an average reduction of 50% of the CO emissions is estimated by applying the innovative combustion control system developed in this work.

Experimental setup

The experimental setup is composed by an inline, 4-cylinder, GDI TC engine, and the main features are reported in Table 1.

Table 1. Engine characteristics.

Displaced volume	1389.9 cc
Stroke	75.6 mm
Bore	76.5 mm
Connecting Rod	144 mm
Compression ratio	10:1
No. of valves per cylinder	4

The engine is equipped with a piezoelectric in-cylinder pressure sensor for each combustion chamber and the signals are recorded with a sampling frequency of 200 kHz. The Alma Automotive mASTRO charge amplifier and the OBI indicating system (provided by the same manufacturer) are used in this experimental setup. The pressure sensor used is from Kistler, and the main features are reported in Table 2.

Table 2. In-cylinder pressure sensor characteristics.

Pressure range	0 to 250 Bar
Overload	300 Bar
Nominal sensitivity	-37.0 pC/Bar
Natural frequency	>215kHz

The in-cylinder pressure signals are used to calculate all the main combustion and knock indexes. Importantly, the MFB50 is calculated from the cumulative net heat release estimated from the low-passed-filtered curves, with a cut-off frequency of 3 kHz. For abnormal combustions, many indexes can be used to estimate the knock

intensity. In this work MAPO is considered and it is evaluated from the following equation:

$$MAPO = max(|p_{filt}|) \quad (1)$$

Where p_{filt} is the bandpass filtered in-cylinder pressure signal. The cut-off frequencies are 5 and 25 kHz.
The exhaust gas temperature at the turbine inlet is measured using a thermocouple and the main features of such sensor are reported in Table 3.

Table 3. Thermocouple characteristics.

Type	K
Diameter	3 mm
Accuracy	± 2.2°C

The thermocouple measurement chain is composed of a National Instruments Compact-Rio 9024, with the module 9213 that works with a sampling frequency of 100 Hz. Due to the sensor dynamics, the comparison between the reference temperature (the values recorded with the production calibrations), and the values sensed during the tests with the combustion controller are always performed considering the thermocouple signal. In other words, even if such sensor is affecting the temperature measurement, since the comparison is always carried out between the signals coming from the same thermocouple, the presented results can be considered robust.
All the modelled engine variables are calculated for the mean cylinder, and they are shown with normalized values for confidentiality reasons. An important aspect to highlight in this work, is that the engine load is referred to the trapped air mass and not to the effective torque at the crankshaft.

A simplified scheme with the main sensors and actuators used for the experimental setup is shown in Figure 1. An oxygen sensor mounted before the catalyst is used for the λ measurement and mixture control. A modified production Engine Control Unit (ECU) has been used, allowing to overwrite some calibration parameters in RT during the tests by communicating the SA via Controller Area Network (CAN) and the target λ value with a voltage signal. The hardware used to communicate the mentioned target calibrations to the ECU is a Simulink Real Time device where the combustion control system is deployed. The RCP device is also connected via CAN to the indicating system to receive the instantaneous combustion and knock indexes. The scheme of the hardware layout used for is reported in Figure 2.

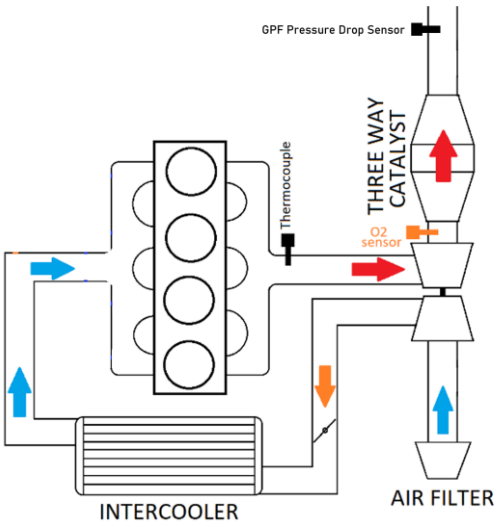

Figure 1: Simplified scheme of the experimental setup.

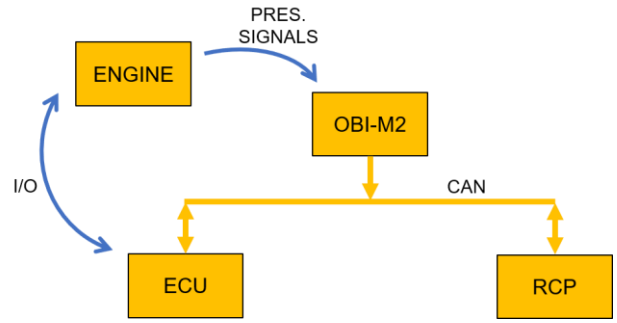

Figure 2: Functional layout of the communication loop.

The mentioned engine is tested carrying out spark sweep tests on the entire operating field, applying different $\boldsymbol{\lambda}$ values. The points highlighted (in cyan rectangle) in Figure 3, which correspond to the high load and speed region of the operating field, are the ones used to calibrate the GT-Power combustion model for the estimation of the pollutant emissions. This model is calibrated only in this region because the experimental validation of the SA- $\boldsymbol{\lambda}$ control system is carried out with transient maneuvers performed in the highlighted part of the operating field.

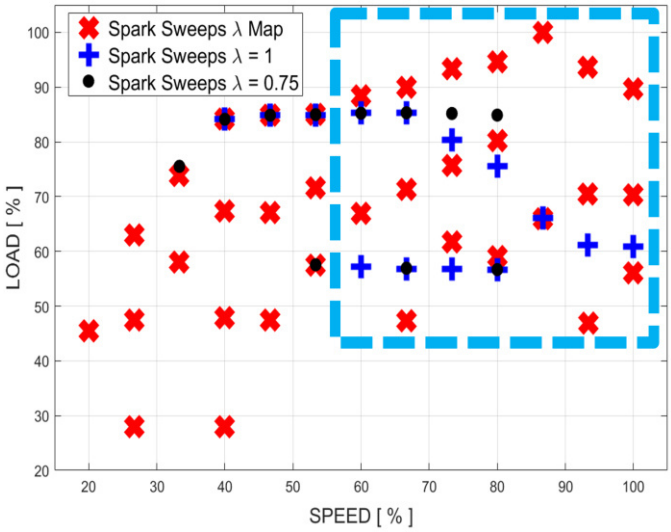

Figure 3. Engine operating points tested for the calibration of the GT-Power combustion model.

Control Development

In this section, the control system that manages both the SA and the λ value to control the knock and the exhaust gas temperature at the turbine inlet is first developed, describing how the exhaust gas temperature at the turbine inlet model [20] is reversed and then it is offline validated using a SiL approach.

Conversion of the exhaust gas temperature model into a model-based λ controller

The λ control system is based on the exhaust gas temperature model proposed in [20]. The complete calculation chain, starting from the engine control parameters, is explained as follows:

- Based on engine speed, load and λ an FNN-based MFB50 model estimates the combustion phase index. This model is based on the Wiebe parameters obtained after the calibration

of a 0D combustion model carried out with a self-developed optimization algorithm [19, 20].

- Using the engine speed, the load, the λ value, and the MFB50 the TEVO is calculated with an analytical model.
- Finally, the TEVO is converted into the exhaust gas temperature value measured in different points, such as in the exhaust runners and the turbine inlet. The analytical function used to convert the TEVO value, called ΔT model, takes as input the MFB50, the engine speed and the load.

The λ control algorithm based on the reversed exhaust gas temperature model consists of an open loop calculation chain, that estimates in a fast way the value to reach the target value of the exhaust gas temperature, and a closed loop part, that adjusts the open loop calculation using the feedback coming from the in-cylinder pressure sensors. In Figure 4, the open loop chain is shown.

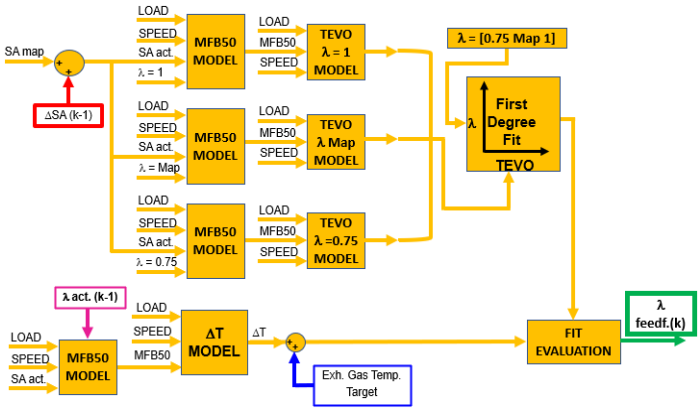

Figure 4. The block scheme of the open loop chain of the λ control system.

The main steps of the algorithm are the following:

- Using the engine speed, the load, the actuated SA (calculated as the sum between the mapped value for the actual operating condition and the SA correction of the previous iteration), and the actuated λ of the previous iteration, the ΔT model calculates the value of temperature to be added to the exhaust gas temperature target value to obtain the TEVO target. It is important to highlight that, since the MFB50 and the ΔT models require as input the SA and the λ values, it is necessary to use the quantities calculated in the previous iteration to obtain the values to be actuated in the current time step.
- Using the same inputs of the ΔT model, the MFB50 one calculates the combustion phase for different λ values ($\lambda = 1$, λ mapped, $\lambda = 0.75$), which are then used to evaluate the TEVO for different λ values.
- While the TEVO model proposed in [20] uses a linear fit to calculate the desired TEVO value, exploiting the λ as independent variable, in this case the axes for the fit evaluation are reversed. Indeed, the linear interpolation which expresses the TEVO – λ dependence is calculated and then used to calculate the target λ value.

The proposed algorithm allows to calculate the target λ value to reach the admissible exhaust gas temperature, but it is necessary to introduce a closed loop chain to compensate the errors of the models. For this reason, the same exhaust gas temperature model is used to estimate the current value, using the measured MFB50 values, and to calculate the error with respect to the target one. Then the error is managed by a PID controller that adjusts the λ value calculated by the open loop chain. The block scheme of the closed-loop algorithm is shown in Figure 5.

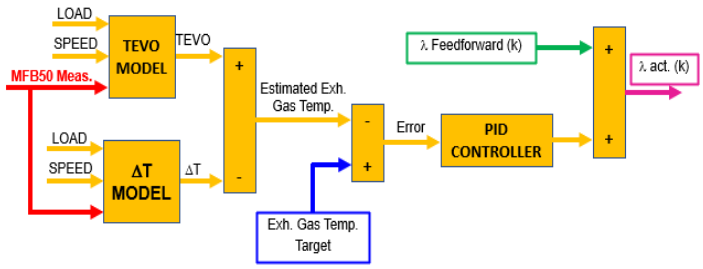

Figure 5. The block scheme of the closed loop chain of the λ control system.

As shown in Figure 6, in the block 5 and 6 the reversed knock model and the reversed PMAX one use the λ value as input. In the first version of the SA control algorithm, these two models used the value calculated from a map as a function of the engine speed and load, while the calculated λ value is used in the following steps. Coupling the SA and the proposed λ control system, the interaction between the two algorithms is that described in Figure 6.

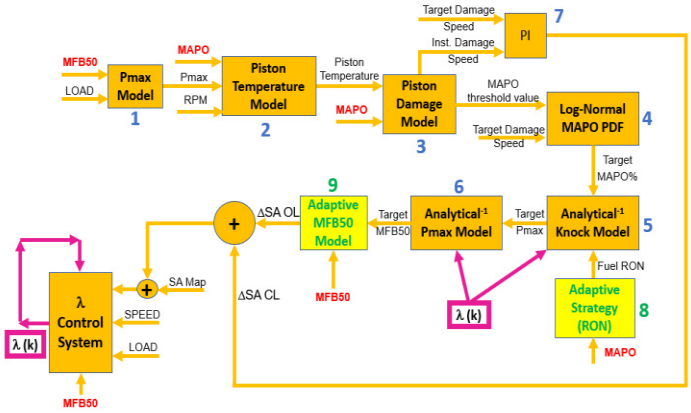

Figure 6. Interaction between the SA and the λ controller.

In the following paragraph the proposed control algorithm is tested in Simulink before deploying it in the Simulink Real Time-based, RCP system to control the engine at the test bench.

Software-in-the-loop validation

Before using the developed SA–λ control system to directly manage the engine at the test bench, the complete algorithm has been tested in Simulink by coupling it with the engine simulator described in [30]. In the following figures, the implementation in Simulink of the complete Software in the loop system is shown. Figure 7 shows the complete SiL environment where the engine simulator (Figure 8) and the control system (Figure 9) are coupled together.

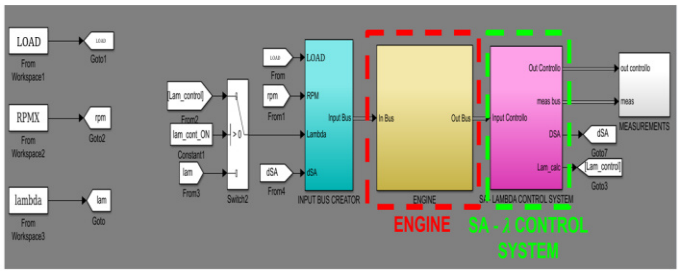

Figure 7. Simulink model of the simulator developed to validate the SA - λ controller.

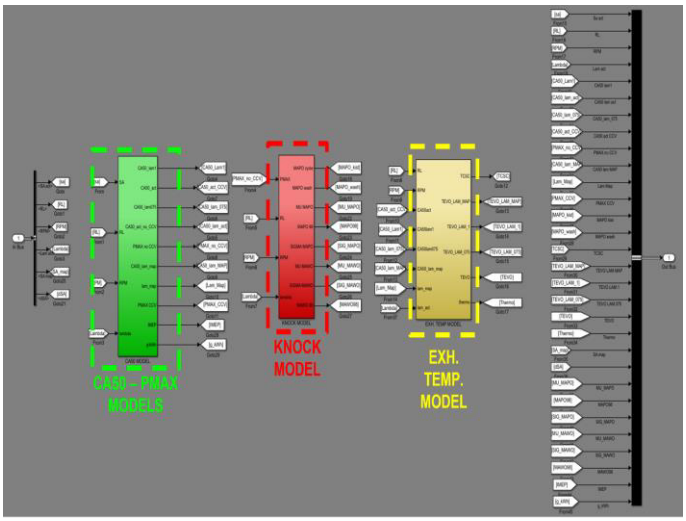

Figure 8. Simulink model of the engine model previously developed by the authors.

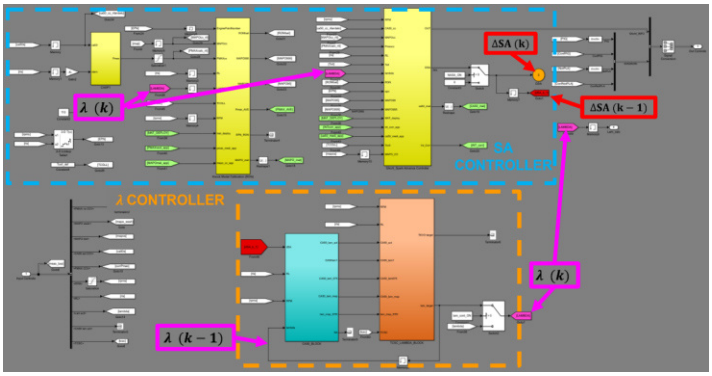

Figure 9. Simulink model of the SA - λ control system.

The validation is carried out using two different transient profiles. The main characteristics of these two profiles are:

- In the first one (Figure 10), the engine is managed automatically by the test bench control system to move from a low load condition to the wide-open throttle in 10 seconds and at the same time, the engine speed increases to reach the maximum value. Nevertheless, it cannot be compared to a real speed and load trend followed in a real maneuver carried out on the track or during an aggressive Real Driving Emissions (RDE) cycle.
- The second profile (Figure 13) is representative of a real track maneuver, where the engine passes from low load conditions to the maximum values in 4 seconds.

In Figure 11, the results related to the simulation carried out for the first transient profile are shown. It is important to highlight that both the simulations related to the two different tests (Transient Test 1 and Transient Test 2) are carried out imposing a Research Octane Number (RON) value equal to 95, and an intake air temperature equal to 35 C°.

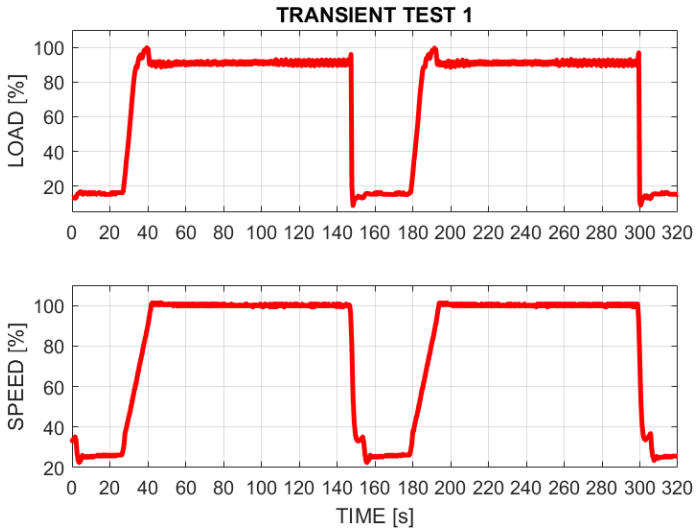

Figure 10. Speed and load profiles related to the transient test 1 for the offline SA – λ control system validation.

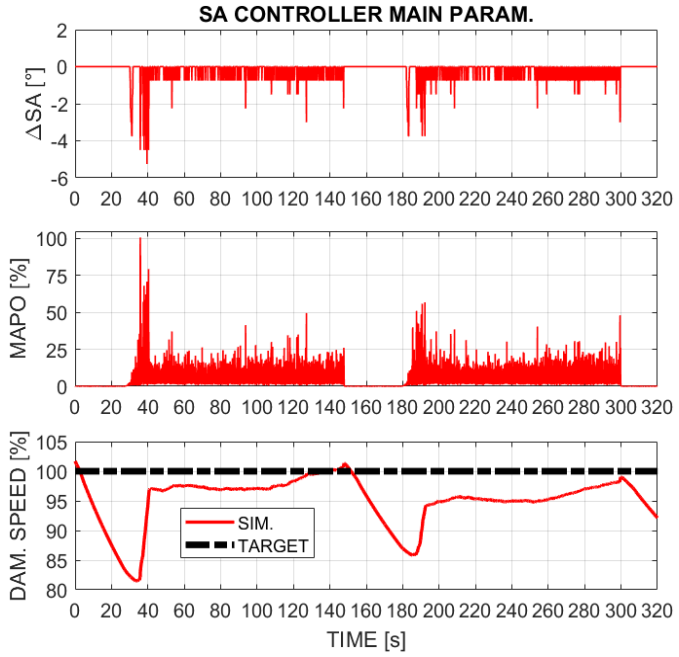

Figure 11. SA correction applied by the control system, percentage cyclic MAPO values, and the calculated damage speed during the transient test 1.

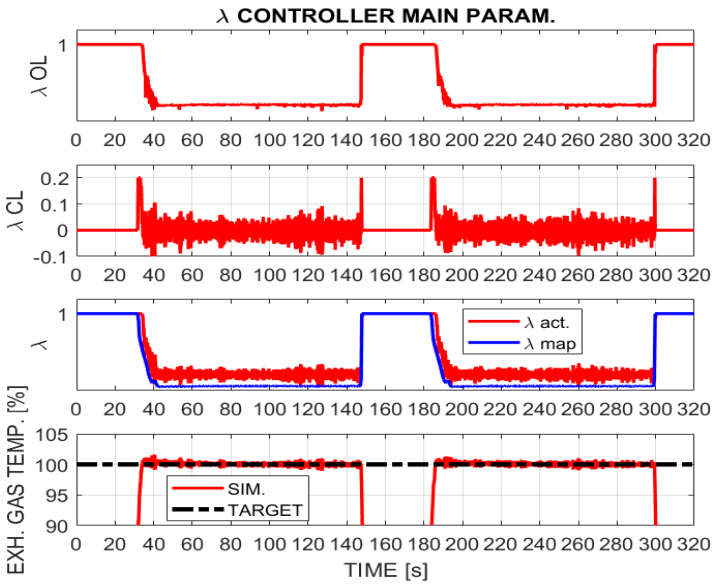

Figure 12. Main λ controller parameters during transient test 1.

As it is possible to see from the last subplots of Figure 11 and 12, the control system can manage the SA and the λ values to achieve the target damage speed and the target exhaust gas temperature, which is the maximum value admitted at the turbine inlet. In Figure 12, the quantities reported are listed below:

- The λ value calculated by the open loop chain ($\lambda\ OL$).
- The corrective λ value calculated by the closed loop chain ($\lambda\ CL$).
- The comparison between the actuated λ value and one calculated with the production map of the engine
- The unfiltered exhaust gas temperature, and the graph is zoomed on the area where the controller works.

The same results are reported in Figure 14, for the second simulation, i.e., the transient test 2.

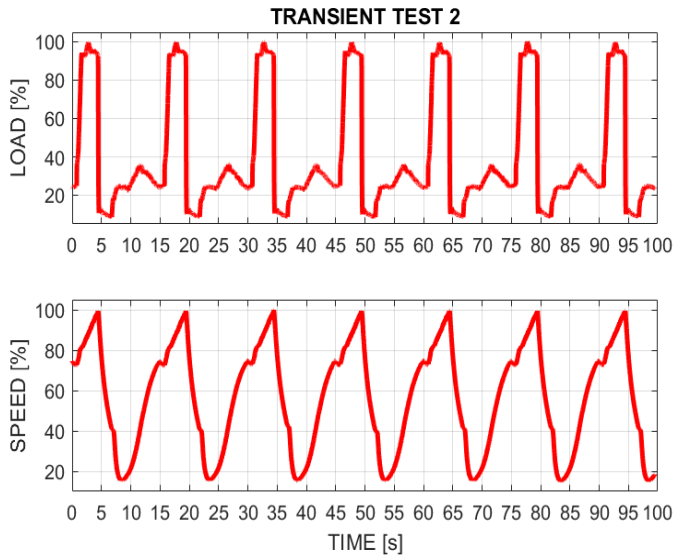

Figure 13. Speed and load profiles related to the transient test 2 for the offline SA – λ control system validation.

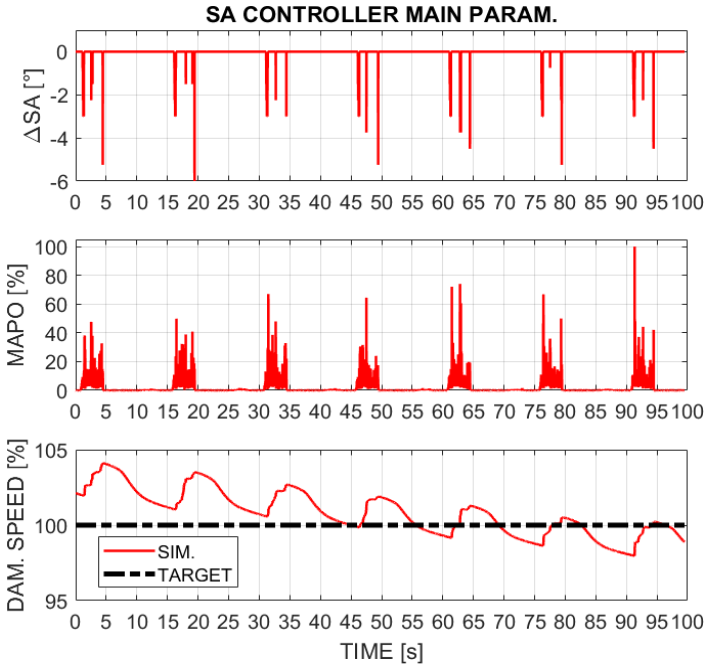

Figure 14. SA correction applied by the control system, percentage cyclic MAPO values, and the calculated damage speed during test 2.

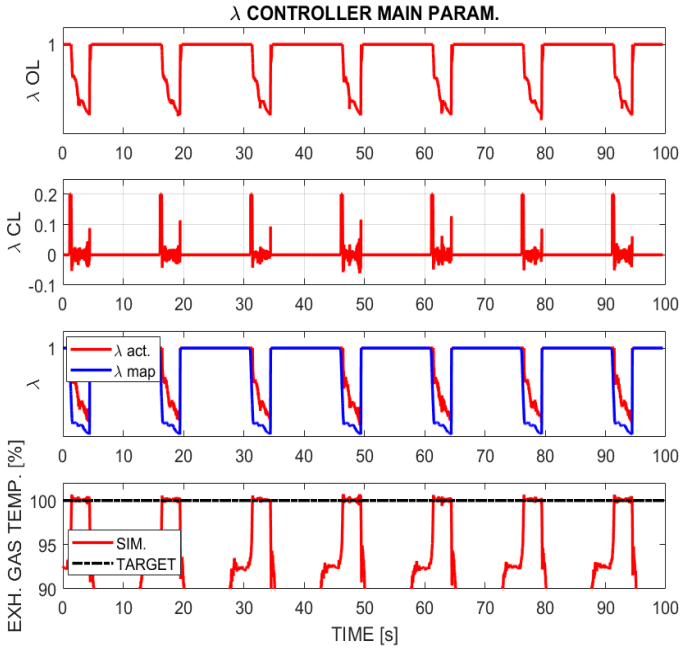

Figure 15. Main λ controller parameters during transient test 2.

The results demonstrate that the developed combustion control system allows to manage the SA and λ values under transient conditions, respecting the imposed damage speed and the maximum admissible exhaust gas temperature. To better understand how the controller manages the exhaust gas temperature during the transient profile, in Figure 16 the simulated exhaust gas temperature obtained for the

transient shown in Figure 10 with the production SA and λ maps is compared to the one calculated with the activated SA – λ control.

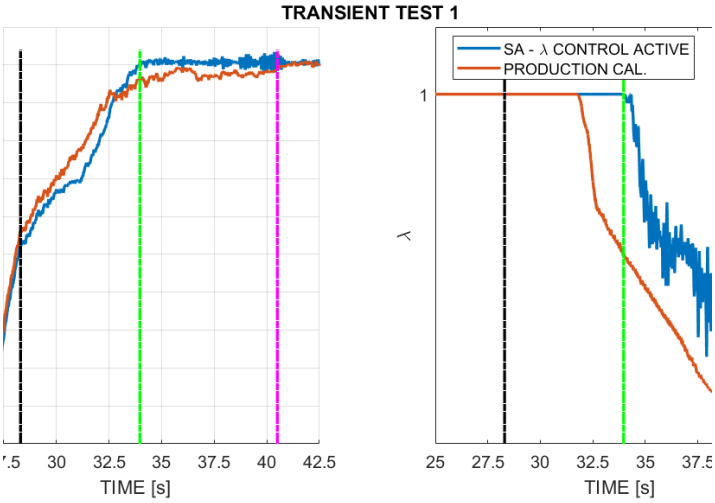

Figure 16. Comparison between the unfiltered exhaust gas temperature measured with the production calibrations and with the activated SA – λ controller (left-hand graph) and the actuated lambda profiles (right-hand graph).

The trend of the exhaust gas temperature profile in Figure 16 can be divided and analyzed into different parts:

- From 27.75 seconds to 33 seconds the SA controller manages the spark timing to target the imposed damage speed, and at the same time the lambda controller keeps the stoichiometric air-to-fuel ratio value.
- From 33 seconds to 41 seconds, the SA and the λ value are both controlled to run the engine contemporarily under knock-limited conditions and with the admissible exhaust gas temperature at the turbine inlet.
- From 41 seconds, the engine operates at the maximum speed and load conditions, and the exhaust gas temperature at the turbine inlet reaches the limit also with the production calibrations (brown line).

Finally, an interesting analysis can be carried out superposing the efficiency gain as a function of the engine speed and load breakpoints measured during the two transient tests (for the operating conditions where the knock and the component strategies are critical), as shown in Figure 17. This efficiency map is obtained with an offline simulation carried out for the steady state conditions, optimizing the SA and λ to run the engine under knock limited operating conditions and with the maximum exhaust gas temperature.

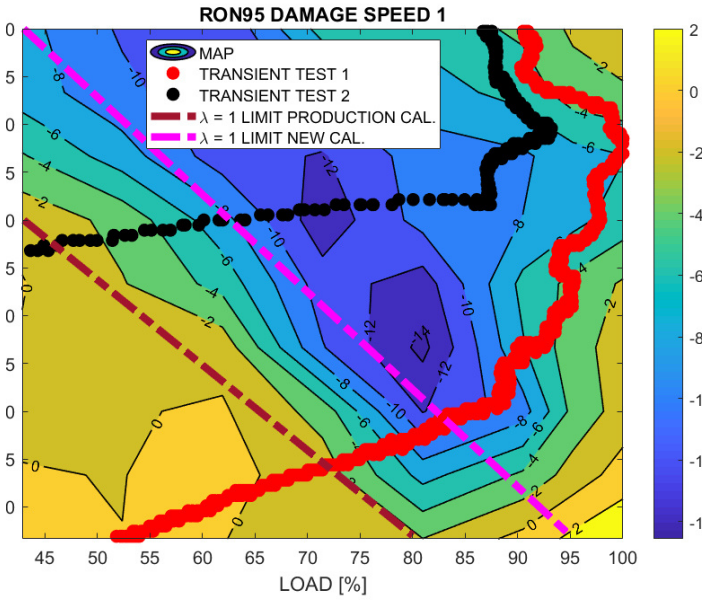

Figure 17. Engine operating conditions related to transient test 1 and 2 on the ΔBSFC map obtained with the damage speed 1 and RON95 gasoline.

In Figure 17 the limit condition referred to the production calibrations and the new limit obtained by applying the proposed calibration method are shown. Analyzing this figure, some observations can be carried out:

- Since the transient test 2 is three times faster than the transient test 1, the turbo lag effect does not allow to reach the full load condition.
- Considering the distance between the two $\lambda = 1$ limit for the operating conditions reached during the two different tests, the stoichiometric range can be further extended during the second one, i.e., transient test 2.
- As already mentioned earlier, the transient test 2 represents real driving maneuvers (i.e., fast, and aggressive transients), most of the operating points are in the zone of high engine speeds and loads. These conditions allow to use more aggressive calibrations thus leading to maximum increase of efficiency, i.e., the ΔBSFC is minimum (i.e., around -12%). Instead, the transient test 1 is a slow test and has a much wider time where the engine speed and load are maximum (above 95%). In this case, since the engine remains knock limiting conditions for a larger period, the knock and the exhaust gas temperature at turbine inlet become more stringent limitations, and the controller is forced to apply less aggressive calibrations, there-by lowering the efficiency gain to about -4 to -5%.

Experimental validation under steady-state conditions

Once the SiL validation of the controller is completed, the SA – λ control system is implemented in the RCP hardware to directly manage the spark timing and the target λ value. The hardware layout used is the one shown in Figure 2. The target SA is communicated to the production ECU using the CAN protocol, while the target λ value is communicated by generating a voltage signal in the range of 0 – 5 V that is proportional to the controller parameter. This voltage signal is

supplied to the ECU through the connector of the sensor used to measure the pressure drop between the inlet and the outlet of the Gasoline Particulate Filter (GPF), which is not present in the test cell. The scheme of the ECU function that converts the raw electrical input into the corresponding λ value cannot be disclosed for confidentiality reasons, but once it is known the target lambda value can be controlled in a proper way.

The developed SA – λ control system is validated at the test bench carrying out a torque and power curve and then the results are compared to that achieved with the production calibrations. In Figure 18, the results are reported showing the main normalized performance indexes, such as the power and the BSFC. The torque and power curves are measured in both cases with the RON95 gasoline.

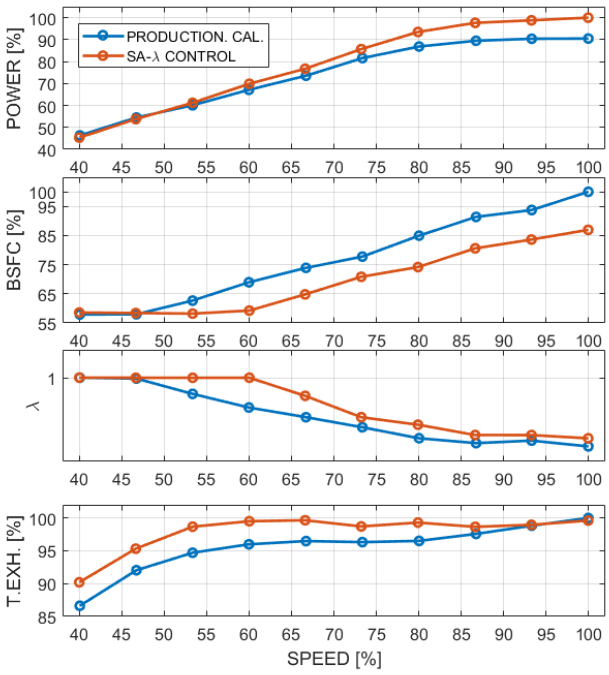

Figure 18. Comparison between the main performance indexes of torque-power curve tests performed with the production calibrations and with the activated SA – λ control system.

Analyzing the graphs, some aspects can be highlighted:

- With the activated SA–λ control system it is possible to increase of about 10 % the power with respect to the production calibrations.
- The BSFC can be reduced by 15% at the maximum speed, i.e., the engine efficiency can be increased by the same value.

As shown in the last graph of Figure 18, the SA–λ controller manages the exhaust gas temperature to keep the exhaust gas temperature close to the maximum value for the operating conditions in which this value can be reached. Indeed, for engine speed conditions lower than 50% the maximum limit cannot be reached applying the stoichiometric air-to-fuel ratio and the knock limited SA.

Experimental validation under transient conditions

The developed SA–λ control system is also tested and validated reproducing transient maneuvers at the test bench. In particular, the engine is controlled reproducing the load and speed profile shown in Figure 13, i.e., reproducing the transient test 2.

The aim is to reproduce the exhaust gas temperature profile at the turbine inlet measured during the same transient maneuver performed with the production calibrations. Considering that the transient test is a fast maneuver during which the engine remains at full load for 3 seconds and due to the slow transient behavior of the thermocouples, it is not possible to set as target or feedback the measured temperature profile during the test with the production calibrations. Indeed, since the maneuver starts from low engine load conditions (i.e., with quite low exhaust gas temperature), the measured exhaust gas temperature at the turbine inlet would remain lower than the maximum admissible value, i.e., the SA–λ control system would always apply the stoichiometric air to fuel ratio. For this reason, the values used as target in the λ control system are the measurements carried out under steady-state conditions and full-load during a power curve carried out with the production calibrations. Thus, the exhaust gas temperature target consists in an array that contains the values at the turbine inlet under full-load conditions as a function of the engine speed.
It is important to highlight the conditions with which the SA–λ control system is tested under transient conditions, which are listed below:

- The transient test is carried out with the RON98 gasoline.
- The test has been carried out once the intake manifold air temperature is under steady-state conditions and close to the reference value. A lower intake manifold air temperature would mean a lower knock tendency, and thus the possibility to reduce more the mixture enrichment to protect the turbine.

The transient maneuver is repeated also with the production calibrations and controlling only the SA to quantify the efficiency gain associated to each variable. Also, these two tests are repeated with the same conditions described above.

In Figure 19 the main quantities measured with the bench system, such as the torque, the power and the exhaust gas temperature at the turbine inlet are reported.

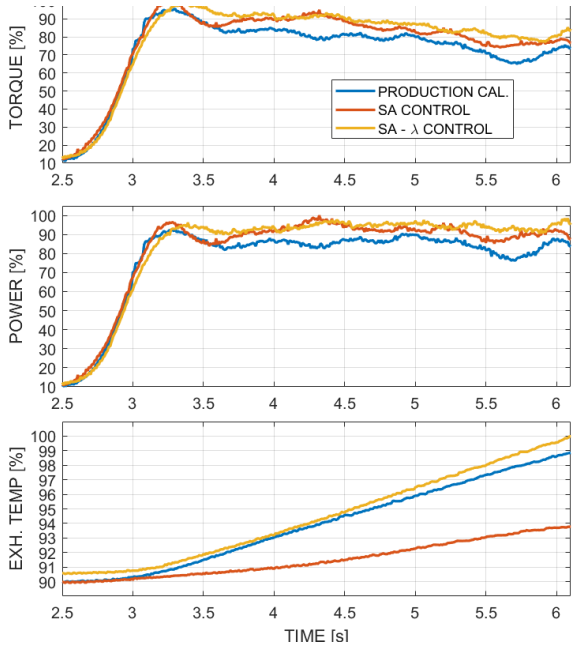

Figure 19. Comparison between the main performance indexes measured during the transient test with the production calibrations, controlling only the SA and both the SA and λ.

The mean values of the torque measured in the full load part of the test are shown in Table 4 to better understand the difference in terms of performance gain associated to each controlled parameter.

Table 4. Comparison between the average torque values sensed under full load conditions during the transient test with the production calibrations, controlling only the SA and both the SA and the target λ.

CONFIGURATION	TORQUE [%]
Production calibrations	89.9 %
SA control	96.5 %
SA – λ control	100 %

Considering the last graph of Figure 19, it is possible to notice that the trend of the exhaust gas temperature at the turbine inlet for the "SA–λ control" test is close to the values measured with the production calibrations. Indeed, the maximum difference is close to 1%. Moreover, Figure 20 shows the difference in terms of C ° between the exhaust gas temperature profiles measured with the production calibrations and the tests carried out with the activated SA–λ control.

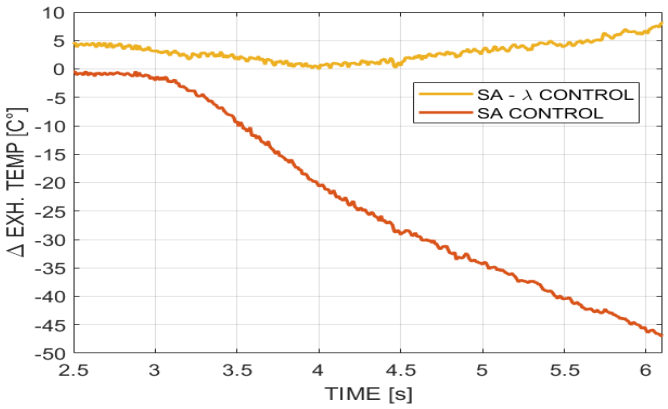

Figure 20. Difference between the exhaust gas temperature profiles measured during the "SA control" test and the "SA-λ" control test with respect to the one carried out with the production calibrations.

The trend related to the "SA – λ control" test has a maximum point lower than 10 C°. Considering the dynamic response of the thermocouples, i.e., similar to a first order system, it can be stated that the quantities that excite the system are equivalent if the differences between the measured dynamic responses are negligible. Thus, it can be stated that the SA–λ control system can properly manage the combustion because it can target the desired damage speed and, at the same time, the exhaust gas temperature profile at the turbine inlet remains close to the value measured with the production calibrations.

As it is demonstrated that the developed control system can properly control the engine, it is possible to compare other important quantities measured during the tests such as the MFB50 and λ. It is important to highlight that the MFB50 profiles are normalized with respect to the minimum value, and thus the units are ΔMFB50. The MFB50 values are recorded with the bench system, that samples the combustion indexes on the CAN bus with a frequency of 100 Hz, and each profile refers to the average cylinder.

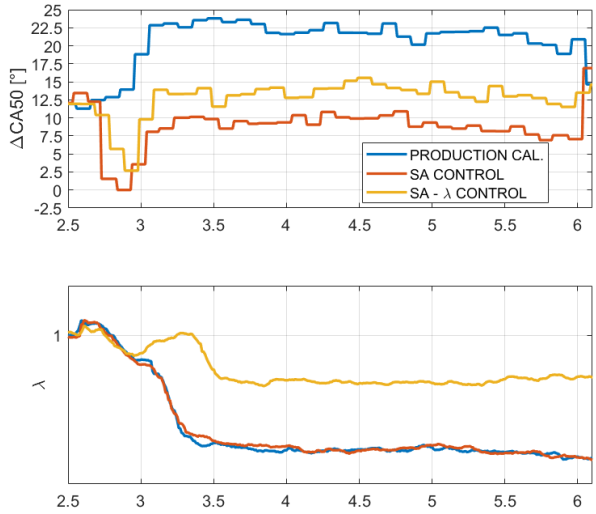

Figure 21. The MFB50 and λ profiles measured during the different transient tests.

The efficiency gain related to the test with both the SA and λ values controlled by the algorithm is evaluated by comparing the results with the reference associated to the production calibrations in terms of BSFC. While the values reported in Figure 18 are those measured during the power curve, the fuel consumption measurement is not reliable under transient conditions because a fuel mass measuring system is used for sensing the gasoline flow. For this reason, a model-based approach is applied to estimate the trapped air mass and thus the BSFC, the measured λ profile and the power. In Figure 22 the percentage BSFC difference achieved during the tests carried out with the production calibrations and with the activated SA–λ control system is reported in the load - speed domain.

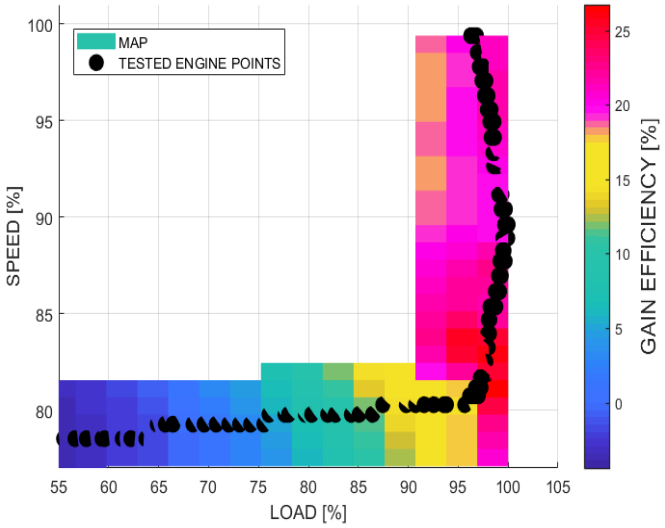

Figure 22. Efficiency increase achieved during the "SA - λ control" test with respect to production calibrations. The black dots represent the engine points touched during the test.

In the previous graph the boosted field starts from the 55 % of the load and, starting from this condition, the gain efficiency becomes positive because the SA–λ control system manages the two parameters to target the desired piston damage speed and the maximum exhaust gas temperature at the turbine inlet, achieving an efficiency increase close to 20 % for the wide-open throttle conditions.

Finally, it is demonstrated that the developed control system can properly manage the combustion enabling a higher combustion efficiency with respect to the production calibrations.

GT-Power model calibration and pollutant emissions estimation

In this paragraph a GT-Power model is calibrated to estimate the effect of controlling the combustion with the developed SA-$\boldsymbol{\lambda}$ combustion control system on the NOx and CO emissions. Indeed, in the experimental setup no system is present for the pollutant emission measurement. The GT-Power model is implemented and calibrated considering the following hypothesis:

- The combustion model refers to the average cylinder. This means that it can reproduce the average in-cylinder pressure curve measured for all the tested operating condition.
- The heat release is modelled using the Wiebe equation. Indeed, the calibration of a predictive combustion model requires some specific geometrical data of the engine, such as the geometry of the intake and exhaust systems, the valves geometry and the data related to the shape of the combustion chamber.
- A two zones combustion model is used. Indeed, the pollutant emissions formation happens in the post-flame gases and thus it is necessary to use at least a two zones model.
- Since no geometrical data of intake and exhaust ducts are available, and thus the intake and the exhaust process cannot be properly validated, the combustion model is calibrated with a closed valves pressure analysis [33]. This means that the trapped air and fuel masses are imposed using the experimental data. Moreover, also the percentage of the Exhaust Gas Recirculation (EGR) is imposed at the beginning of the cycle using a map-based approach thanks to experimental data provided by the engine manufacturer.

The Design Optimizer of GT-Power [31] is used to calibrate the Wiebe parameters and the heat transfer algorithm to match the experimental average pressure curve for each engine operating condition. In particular, the software [33] allows to set different values that are used in an object function minimized by the optimization algorithm to reach the corresponding experimental values. In this case the experimental MFB10 and the PMAX are used as target values to calculate the error of the modelled in-cylinder pressure curves.

In Figures 24 and 25 the simulated and the average experimental in-cylinder pressure curves are compared for different operating points to demonstrate that the combustion model is well calibrated.

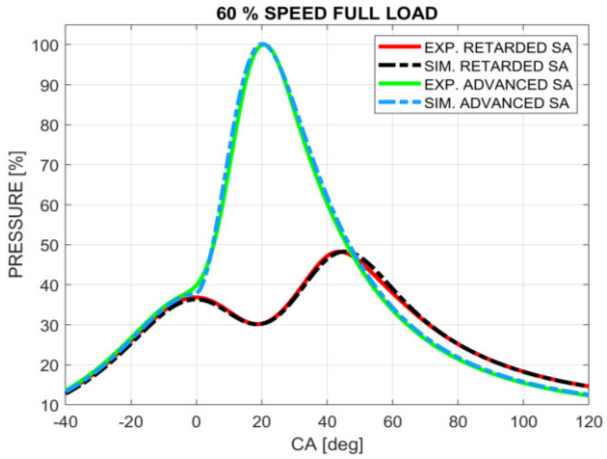

Figure 24. Experimental and simulated in-cylinder pressure curves for the most retarded and the most advanced SA values tested at 60 % of engine speed and full load.

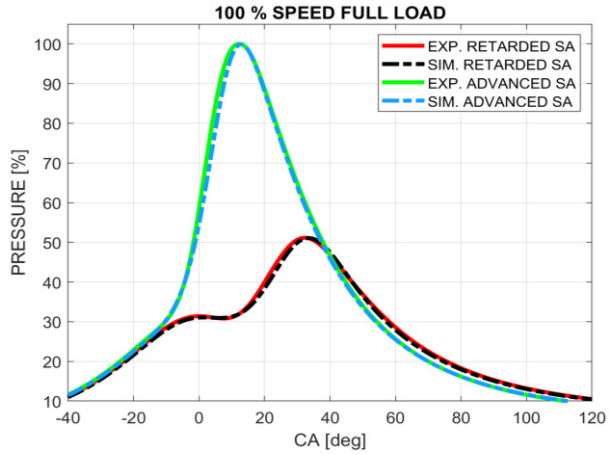

Figure 25. Experimental and simulated in-cylinder pressure curves for the most retarded and the most advanced SA values tested at 100 % of engine speed and full load.

With the calibrated combustion model is possible to calculate the NOx and CO concentration at the exhaust valve opening. In particular, the extended Zeldovich model is implemented in GT-Power for the NOx estimation. As is well-known from the literature, its concentration mainly depends on the maximum in-cylinder temperature reached within the combustion chamber [31, 32]. The considered thermodynamic parameter depends on the load, the combustion phase, and the $\boldsymbol{\lambda}$ value [32]. Moreover, also the engine speed affects the maximum in-cylinder temperature, keeping constant the other engine parameters, because the percentage of EGR increases for higher speed values [33]. Considering these aspects, the NOx values calculated with the 0D combustion model are used to train a FNN algorithm which uses as inputs the load, the MFB50, the $\boldsymbol{\lambda}$ value and the engine speed. The CO model is based on the following oxidation reaction, as proposed by several authors [34, 35]:

$$\boldsymbol{CO + OH \leftrightharpoons CO_2 + H} \qquad (2)$$

During the combustion, this reaction does not proceed following the chemical equilibrium, but it is kinetically driven [29, 31, 32, 34]. In literature the factor $\boldsymbol{\alpha_{CO}}$ is introduced, that represents the CO oxidation

quenching (it can be demonstrated that $\alpha_{CO} > 2$ means that the chemical reaction is quenched):

$$\alpha_{CO} = -\tau_{CO}\left(\frac{B}{T^2} - \frac{1}{4T}\right)\left(\frac{dT}{dt}\right) \quad (3)$$

Where τ_{CO} is the characteristic timescale related to the CO production, B is a constant value, T is the in-cylinder temperature and $\frac{dT}{dt}$ the cooling rate of the gas. It is important to highlight that τ_{CO} depends on the temperature and the OH molar fraction in partial equilibrium conditions [34, 37, 38].

Finally, it can be stated that the CO production depends mainly on the in-cylinder temperature and the cooling rate [34], thus the main engine parameters that affects the production of this pollutant emission are the load, the combustion phase and the λ value, as well known from the literature. Moreover, since the cooling rate can be represented in the angular domain with the following equation:

$$\frac{dT}{dt} = \frac{dT}{d\vartheta}\omega \quad (4)$$

This aspect is demonstrated in Figure 26 where the simulated CO values for different engine speed values, but fixed load and λ, are shown as function of the maximum in-cylinder temperature and the cooling rate (average value calculated during the expansion phase expressed in logarithmic scale).

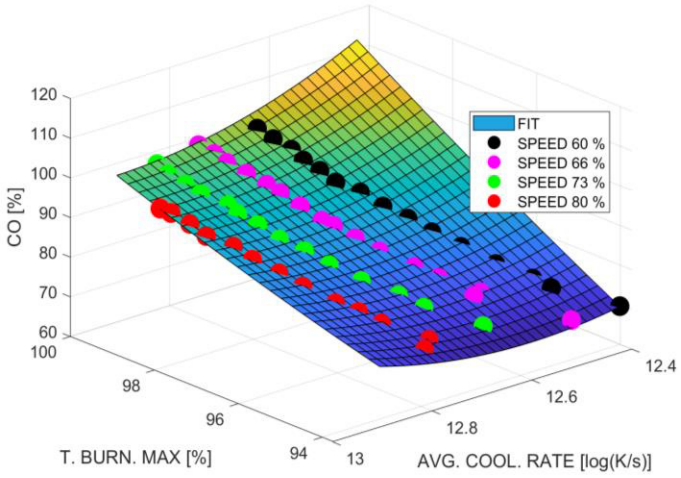

Figure 26. Simulated CO at the exhaust valves opening as function of the maximum in-cylinder temperature the cooling rate for different engine speed values and fixed load and λ value.

Considering these analyses also for the CO emissions, a FNN model is trained using as inputs the load, the MFB50, the λ value and the engine speed. Both the NOx and CO FNN algorithms are trained using an automatic procedure developed and explained by the authors in [30]. In the following figure the accuracy of the two FNN models are shown for the test dataset.

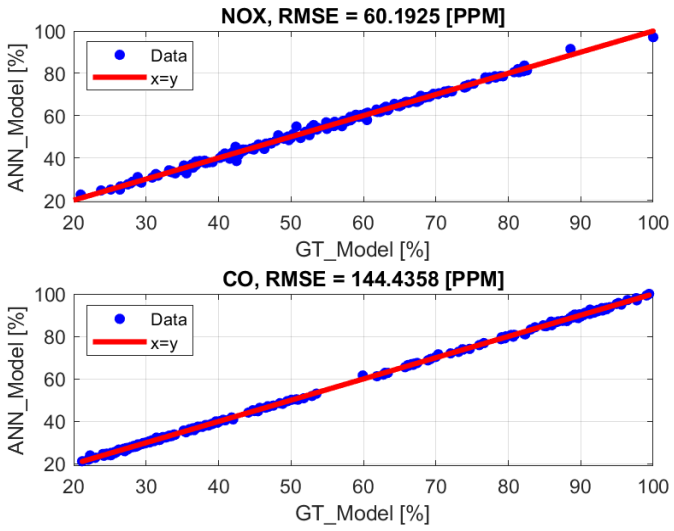

Figure 27. Correlation analysis referred to test dataset between the NOx and CO values calculated with the calibrated GT-Power model and the values calculated with the FNN algorithms.

Thanks to the calibrated FNN-based NOx and CO models it is then possible to easily estimate the effect on the emissions using the engine data measured during the transient tests carried out with the production calibrations and the activated SA–λ control system. In the following figures analyses equivalent to the one shown in Figure 22 are reported for both the estimated NOx and the CO.

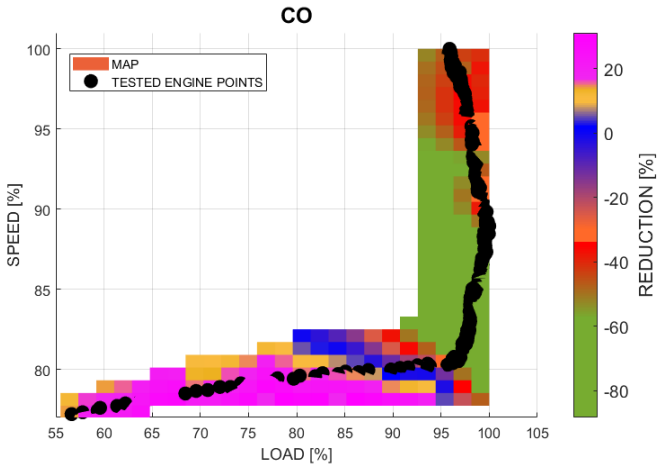

Figure 28. CO percentage difference achieved during the "SA - λ control" test with respect to standard calibrations. The black dots represent the engine points touched during the test.

Analyzing Figure 28 it can be stated that until 90% of the engine load the CO increases because the SA–λ control system applies a more advanced SA value, i.e. incresing the maximum in-cylinder temperature, to run the engine under knock limited conditions and the λ value is stoichiometric during both the tests. In the range between 80% and 85% of engine speed in full load conditions the CO is reduced of 60-80% because the SA–λ control system applies the stoichiometric value, while the λ value applied during the production calibrations test is rich. Finally, in the range between 85% and 100% of engine speed the CO reduction is close to 40% because the SA–λ control system

increases the SA and at the same time reduces the mixture enrichment with respect to the production calibrations.

In Figure 29 the same analysis of Figure 27 is shown for the NOx. In this case the pollutant emission increases with respect to the production calibrations because advancing the SA and reducing the fuel enrichment cause higher maximum in-cylinder temperature. Nevertheless, considering that in the full load region the λ value is still rich also with the activated SA–λ control system, the Three-Way Catalyst (TWC) can convert the NOx with the highest possible efficiency.

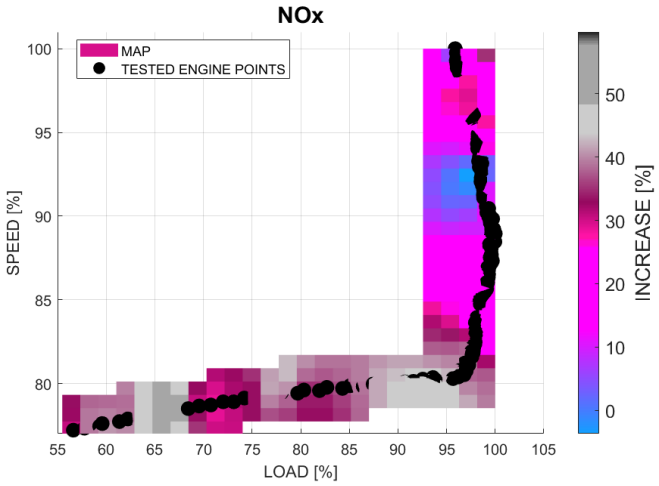

Figure 29. NOx percentage difference achieved during the "SA - λ control" test with respect to production calibrations. The black dots represent the engine points touched during the test.

Conclusions

This work deals with the development and the validation of a model-based combustion control system with which it is possible to manage the SA and λ to increase the efficiency of modern GDI TC engines in the high load and speed range of the operating field, where the SA degradation and the mixture enrichment are typically used to control the knock intensity and the exhaust gas temperature at the turbine inlet.

The developed SA–λ control system is based on the SA control algorithm described in [18] and [19], with which it is possible to control the piston erosion generated by knocking combustion targeting the desired piston damage speed, and on a model-based λ control algorithm developed by reversing the exhaust gas temperature model developed by the authors in [20] and [21]. The complete algorithm is first tested in a SiL environment using a Neural Network based engine simulator developed in [32], demonstrating that the control system can properly manage both the SA and the λ values to run the engine under knock limited conditions and with the maximum admissible exhaust gas temperature at the turbine inlet.

Then, the controller is deployed on a Simulink Real Time-based RCP hardware to directly control the engine at the test bench. First, the SA–λ control system is tested under steady-state conditions carrying out a power curve, and it is demonstrated that the engine efficiency can be increased of about 15 % with respect to the production calibrations. The developed combustion control system is then tested under transient tests, reproducing at the test bench an aggressive RDE maneuver. In this case, it is demonstrated that the engine efficiency can be increased by about 25%. In particular, the efficiency increase achieved under transient conditions is higher because a RON98 gasoline is used, but also because the knock tendency is lower than the one measured under steady-state conditions. Thus, the control system can apply more advanced SA values simultaneously reducing more the mixture enrichment.

In the last part of the work the authors also estimate the effects on the pollutant emissions by using the developed SA–λ control system. Since in the experimental setup no measurement system for the pollutant emissions is available, a GT-Power, Wiebe based, two-zones combustion model is calibrated to reproduce the average in-cylinder pressure curve measured for each operating conditions tested. In this way, the NOx can be estimated using the Zeldovich model, while the CO is calculated using the kinetical models implemented in GT-Power. Then, the simulated results of pollutant emissions are used to train two FNN models thanks to which it is possible to estimate the desired values with a low computational effort using the engine parameters measured during the transient test. A reduction of about 50 % of CO emission with respect to the production calibrations of the engine is estimated for the high load and speed region of the operating range with an increase of 20% of NOx. These results can be described considering that, running the engine under knock limited conditions, and reducing the mixture enrichment, the maximum in-cylinder temperature increases leading to a higher NOx production. Nevertheless, the TWC can convert this pollutant emission with the maximum efficiency because the final applied λ value is still rich in the high load and speed part of the operating field.

The developed SA–λ control system can properly work with robust feedback from the combustion chamber. Nevertheless, it is well known that the in-cylinder pressure sensors cannot be used for the final on-board application. For this reason, future works will be the tests of the proposed control system using an innovative and cheap piezoelectric washer sensor that can be installed between the engine head and the spark plug [39, 40].

References

1. Nathalie Barbosa Reis Monteiro, Elaine Aparecida da Silva, José Machado Moita Neto, “Sustainable development goals in mining”, Journal of Cleaner Production, Volume 228, 2019, Pages 509-520, ISSN 0959-6526, https://doi.org/10.1016/j.jclepro.2019.04.332.
2. DieselNet, “Emission Standards: Summary of worldwide engine and vehicle emission standards,” DieselNet, accessed May 2021, https://dieselnet.com/standards/
3. AVL Public Discussion, https://www.avl.com/documents/4329920/48266926/AVL+Emission+Test+System+and+Emission+New+Regislation.pdf,17/11/2021.
4. Kalghatgi, G., Algunaibet, I., and Morganti, K., "On Knock Intensity and Superknock in SI Engines," SAE Int. J. Engines 10(3):2017, doi:10.4271/2017-01-0689.
5. Reif, K., “Gasoline Engine Management, Systems and Components”, Springer Vieweg, 2015, doi:10.1007/978-3-658-03964-6.
6. Szabados, G., Szűcs, H., Hézer, J., Sanders, B. (2022) “Investigation of Possibilities of λ = 1 Full Load Operation for Gasoline Engines in the Light of Future Emission Regulation”, Periodica Polytechnica Transportation Engineering, 50(2), pp. 111–127. https://doi.org/10.3311/PPtr.17433
7. Baumgarten Henning et al., “New lambda = 1 gasoline powertrains new technologies and their interaction with connected and autonomous driving”, Connectivity - key to future emission and consumption reduction? : In vehicle and powertrain : Engine & Environment 2018 : 30th International AVL Conference "Engine & Environment", June 7th-8th, 2018, Graz, Austria, Seiten/Artikel-Nr: 149-164, https://www.avl.com/documents/10138/8684463/14_Baumgarten_hand_out.pdf
8. Gainey, B., Gohn, J., Yan, Z., Malik, K. et al., “HCCI with Wet Ethanol: Investigating the Charge Cooling Effect of a High

Latent Heat of Vaporization Fuel in LTC," SAE Technical Paper 2019-24-0024, 2019, https://doi:10.4271/2019-24-0024.
9. Gao, J., Yao, A., Feng, L., Xu, H. et al., "Experimental Investigation on the Failures of Engine Piston Subjected to Severe Knock," SAE Technical Paper 2019-01-0705, 2019, https://doi.org/10.4271/2019-01-0705.
10. Cavina, N., Rojo, N., Ceschini, L., Balducci, E. et al., "Investigation of Knock Damage Mechanisms on a GDI TC Engine," SAE Technical Paper 2017-24-0060, 2017, https://doi:10.4271/2017-24-0060.
11. L. Ceschini, A. Morri, E. Balducci, N. Cavina, N. Rojo, L. Calogero, L. Poggio, "Experimental observations of engine piston damage induced by knocking combustion", Mater. Des. 114 (2017) 312–325, http://dx.doi.org/10.1016/j.matdes.2016.11.015.
12. E. Balducci, L. Ceschini, N. Rojo, N. Cavina, R. Cevolani, M. Barichello, "Knock induced erosion on Al pistons: Examination of damage morphology and its causes", Engineering Failure Analysis, Volume 92, October 2018, Pages 12-31, https://doi.org/10.1016/j.engfailanal.2018.05.002.
13. Fu, H., Chen, X., Shilling, I., and Richardson, S., "A One-Dimensional Model for Heat Transfer in Engine Exhaust Systems," SAE Technical Paper 2005-01-0696, 2005, https://doi.org/10.4271/2005-01-0696.
14. Fulton, B., Van Nieuwstadt, M., Petrovic, S., and Roettger, D., "Exhaust Manifold Temperature Observer Model," SAE Technical Paper 2014-01-1155, 2014, https://doi.org/10.4271/2014-01-1155.
15. Martin, D. and Rocci, B., "Virtual Exhaust Gas Temperature Measurement," SAE Technical Paper 2017-01-1065, 2017, https://doi.org/10.4271/2017-01-1065.
16. Cavina, N., Cerofolini, A., Corti, E., Ponti, F. et al., "Innovative Techniques for On-Board Exhaust Gas Dynamic Properties Measurement," *SAE Int. J. Engines* 6(1):217-227, 2013, https://doi.org/10.4271/2013-01-0305.
17. Son, S., "Exhaust Gas Temperature Determination with HEGO Parameters," SAE Technical Paper 2010-01-1303, 2010, https://doi.org/10.4271/2010-01-1303.
18. Brusa, A.; Cavina, N.; Rojo, N.; Mecagni, J.; Corti, E.; Ravaglioli, V.; Cucchi, M.; Silvestri, N. Development and Experimental Validation of an Adaptive, Piston-Damage Based Combustion Control System for SI Engines: Part 1—Evaluating Open-Loop Chain Performance. Energies 2021, 14, 5367. https://doi.org/10.3390/en14175367
19. Brusa, A.; Cavina, N.; Rojo, N.; Mecagni, J.; Corti, E.; Moro, D.; Cucchi, M.; Silvestri, N. Development and Experimental Validation of an Adaptive, Piston-Damage-Based Combustion Control System for SI Engines: Part 2—Implementation of Adaptive Strategies. Energies 2021, 14, 5342. https://doi.org/10.3390/en14175342
20. Mecagni, J., Brusa, A., Cavina, N., Corti, E. et al., "Control-Oriented Exhaust Gas Temperature Modelling Based on Wiebe Equation," SAE Int. J. Engines 14(5):2021, https://doi:10.4271/03-14-05-0042.
21. Mecagni, J., Brusa, A., Cavina, N., Ponti, F. et al., "Model-Based Exhaust Gas Temperature Control to Reduce the Mixture Enrichment at High Loads," SAE Int. J. Engines 16(3):2023, https://doi.org/10.4271/03-16-03-0020.
22. Johnson, R., Kaczynski, D., Zeng, W., Warey, A. et al., "Prediction of Combustion Phasing Using Deep Convolutional Neural Networks," SAE Technical Paper 2020-01-0292, 2020, https://doi:10.4271/2020-01-0292.
23. Scocozza, G., Silvagni, G., Brusa, A., Cavina, N. et al., "Development and Validation of a Virtual Sensor for Estimating the Maximum in-Cylinder Pressure of SI and GCI Engines," SAE Technical Paper 2021-24-0026, 2021, https://doi.org/10.4271/2021-24-0026.
24. Maldonado, B., Kaul, B., and Szybist, J., "Artificial Neural Networks for In-Cycle Prediction of Knock Events," SAE Technical Paper 2022-01-0478, 2022, https://doi:10.4271/2022-01-0478.
25. Brusa, A., Cavina, N., Rojo, N., Cucchi, M. et al., "Development and Validation of a Control-Oriented Analytic Engine Simulator," SAE Technical Paper 2019-24-0002, 2019, https://doi.org/10.4271/2019-24-0002.
26. Warey, A., Gao, J., and Grover, R., "Prediction of Engine-Out Emissions Using Deep Convolutional Neural Networks," *SAE Int. J. Advances & Curr. Prac. in Mobility* 3(6):2863-2871, 2021, https://doi:10.4271/2021-01-0414.
27. Brusa, A.; Giovannardi, E.; Barichello, M.; Cavina, N. Comparative Evaluation of Data-Driven Approaches to Develop an Engine Surrogate Model for NOx Engine-Out Emissions under Steady-State and Transient Conditions. Energies 2022, 15, 8088. https://doi.org/10.3390/en15218088
28. Zhang, H., Weyhing, T., Fan, X., Blesinger, G. et al., "Modelling of Engine Cooling System with a New Modelling Approach Based on Dynamic Neural Network," SAE Technical Paper 2021-01-0203, 2021, https://doi:10.4271/2021-01-0203.
29. Jander, B. and Baar, R., "Modeling Thermal Engine Behavior Using Artificial Neural Network," SAE Technical Paper 2017-01-0534, 2017, https://doi:10.4271/2017-01-0534.
30. Shethia, F., Mecagni, J., Brusa, A., and Cavina, N., "Development and Software-in-the-Loop Validation of an Artificial Neural Network-Based Engine Simulator," SAE Technical Paper 2022-24-0029, 2022, https://doi.org/10.4271/2022-24-0029.
31. Michos, K.N. and Bikas, G., "Quasi-Dimensional Multi-Zone Combustion Diagnostic Tool for SI Engines with Novel NOx and CO Emissions Models," SAE Int. J. Advances & Curr. Prac. in Mobility 2(4):1818-1848, 2020, https://doi:10.4271/2020-01-0289.
32. Valério, M., Raggi, K., and Sodré, J., "Model for Kinetic Formation of CO Emissions in Internal Combustion Engines," SAE Technical Paper 2003-01-3138, 2003, https://doi.org/10.4271/2003-01-3138.
33. GT-Power Manual, Engine Performance, 2022.
34. Michos, K.N. and Bikas, G., "Quasi-Dimensional Multi-Zone Combustion Diagnostic Tool for SI Engines with Novel NOx and CO Emissions Models," SAE Int. J. Advances & Curr. Prac. in Mobility 2(4):1818-1848, 2020, https://doi:10.4271/2020-01-0289.
35. S. Bougrine, S. Richard, J.-B. Michel, D. Veynante, Simulation of CO and NO emissions in a SI engine using a 0D coherent flame model coupled with a tabulated chemistry approach, Applied Energy, Volume 113, 2014, Pages 1199-1215, ISSN 0306-2619, https://doi.org/10.1016/j.apenergy.2013.08.038
36. Fagundez, J., Martins, M., and Salau, N., "Comparison of NOx emissions from hydrous ethanol and n-butanol predicted by an Otto cycle two-zone model using the Zeldovich reactions mechanism," SAE Technical Paper 2018-36-0105, 2018, https://doi.org/10.4271/2018-36-0105.
37. Bikas, G. and Michos, K., "Carbon Monoxide Emissions Model for Data Analytics in Internal Combustion Engine Applications Derived from Post-Flame Chemical Kinetics," SAE Int. J. Engines 11(6):947–964, 2018, https://doi:10.4271/2018-01-1153.
38. Internal Combustion Engine Fundamentals, John Heywood, McGraw Hill Professional, 2018
39. Corti, E., Raggini, L., Rossi, A., Brusa, A. et al., "Application of Low-Cost Transducers for Indirect In-Cylinder Pressure

Measurements," *SAE Int. J. Engines* 16(2):213-230, 2023, https://doi.org/10.4271/03-16-02-0013.
40. Brusa, A., Mecagni, J., Corti, E., and Silvestri, N., "Application of a Neural-Network-Based Algorithm for the Real-Time Correction of the In-Cylinder Pressure Signal Sensed with a Piezoelectric Washer," *SAE Int. J. Engines* 16(5):2023, https://doi.org/10.4271/03-16-05-0039.

Definitions/Abbreviations

BSFC	Brake Specific Fuel Consumption
CAN	Controller Area Network
ECU	Engine Control Unit
EGR	Exhaust Gas Recirculation
FNN	Feedforward Neural network
GDI	Gasoline Direct Injection
GPF	Gasoline Particulate Filter
MAPO	Maximum Amplitude Pressure Oscillation
MFB10	10% of the Mass Fraction Burned
MFB50	50% of the Mass Fraction Burned
PMAX	Maximum In-Cylinder Pressure
RCP	Rapid Control Prototyping
RDE	Real Driving Emission
RON	Research Octane Number
RT	Real Time
SA	Spark Advanced
SiL	Software-in-the-Loop
TC	Turbo-charged
TEVO	Temperature at Exhaust Valve Opening
TWC	Three Way Catalyst
UEGO	Universal Exhaust Gas Oxygen
VCR	Variable Compression Ratio